Draft version May 8, 2014
Preprint typeset using LaTeX style emulateapj v. 11/12/01

arXiv:1405.1475v1 [astro-ph.HE] 6 May 2014

THE LIGHT CURVE AND INTERNAL MAGNETIC FIELD OF THE MODE-SWITCHING PULSAR PSR B0943+10

Natalia I. Storch[1], Wynn C.G. Ho[2], Dong Lai[1], Slavko Bogdanov[3], and Craig O. Heinke[4]

Draft version May 8, 2014

ABSTRACT

A number of radio pulsars exhibit intriguing mode-switching behavior. Recent observations of PSR B0943+10 revealed correlated radio and X-ray mode switches, providing a new avenue for understanding this class of objects. The large X-ray pulse fraction observed during the radio quiet phase (Q mode) was previously interpreted as a result of changing obscuration of X-rays by dense magnetosphere plasma. We show that the large X-ray pulse fraction can be explained by including the beaming effect of a magnetic atmosphere, while remaining consistent with the dipole field geometry constrained by radio observations. We also explore a more extreme magnetic field configuration, where a magnetic dipole displaced from the center of the star produces two magnetic polar caps of different sizes and magnetic field strengths. These models are currently consistent with data in radio and X-rays and can be tested or constrained by future X-ray observations.

Subject headings: stars: neutron – magnetic fields – pulsars: individual (PSR B0943+10)

1. INTRODUCTION

It has long been known that many radio pulsars exhibit variabilities in their pulse shapes and intensities, on a wide variety of timescales. These include phenomena such as subpulse drifts, nulls and bursts, and long- and short-term on/off quasiperiodic mode-switching (see Cordes 2013 for a review). Until recently, these variabilities were thought to be due to changes in the radio emission process, not tied to the global properties of the pulsar magnetosphere and high energy emission. However, Kramer et al. (2006) discovered that PSR B1931+24 shows large changes in its spin-down rate, correlated with its mode switching, suggesting that the switching is strongly tied to the global energetics of the pulsar. Later, PSR J1841-0500 (Camilo et al. 2012) and PSR J1832+0029 (Lorimer et al. 2012) were also shown to have similar behavior. A number of other pulsars display smaller changes in spin-down rates which are correlated with changes in their average pulse profiles (Lyne et al. 2010). These may correspond to a less extreme version of "mode-switching".

This connection between radio mode-switching and global magnetosphere change was further strengthened by the simultaneous X-ray and radio observations of PSR B0943+10 (Hermsen et al. 2013; hereafter H13). This is a relatively old pulsar which has been known for a long time to transition from a bright, highly organized radio "on" (B) state to a quieter, more chaotic radio "off" (Q) state on timescales of a few hours (Rankin & Suleymanova 2006). In addition, its radio emission exhibits subpulse drift, which was shown by Deshpande & Rankin (2001) to likely come from 20 'sub-beams' arranged in a conical structure. Deshpande & Rankin (2001) also constrained the emission geometry of the radio beam, demonstrating that the line of sight, rotation axis, and magnetic axis are all nearly parallel, with a misalignment of only $\sim 10^\circ$. H13 found that the radio mode-switching of PSR B0943+10 is correlated with a similar switching in its X-ray emission: during the B mode the X-ray emission is steady and non-pulsed, while during the Q mode the X-ray flux increases by a factor of ~ 2 and becomes highly pulsed.

As PSR B0943+10 is a paragon of mode-switching pulsars, understanding its behavior may provide important insight into the physical origin of pulsar mode-switching. In this paper, we discuss three puzzling aspects of PSR B0943+10's correlated X-ray and radio emission (section 2) and demonstrate that two of them can be resolved through accurate light curve modeling that accounts for the effect of a strong magnetic field (section 3). We consider an alternative, "displaced dipole" magnetic field geometry, and show that it provides a satisfactory explanation for all three puzzles (section 4). In section 5 we summarize our findings, discuss their implications, and propose concrete methods by which they can be refuted or confirmed.

2. OBSERVATIONAL PUZZLES OF PSR B0943+10

Of the several puzzles that PSR B0943+10 presents, the most important is, undoubtedly, the question of *how* and *why* the mode-switching occurs. The physical mechanism for mode change is unknown (see Cordes 2013) and we do not attempt to tackle it directly in this paper. Instead, we address several "smaller" puzzles that arose with the recent simultaneous X-ray and radio observations of this pulsar (H13).

First, the X-ray observation showed that the pulsar exhibits a steady unpulsed emission during the pulsar's radio-bright (B) mode, and a larger, strongly pulsed emission during the radio-quiet mode (Q). The emission during the radio-bright mode is suggested to be non-thermal in nature, while the added pulsed component in the radio-quiet mode is consistent with being thermal (H13). How-

[1] Center for Space Research, Department of Astronomy, Cornell University, Ithaca, NY 14853
[2] Mathematical Sciences and STAG Research Centre, University of Southampton, Southampton, SO17 1BJ, United Kingdom
[3] Columbia Astrophysics Laboratory, Columbia University, 550 West 120th Street, New York, NY 10027
[4] Department of Physics, University of Alberta, CCIS 4-181, Edmonton, AB, T6G 2E1, Canada

ever, the somewhat limited data at present is well fitted by either a blackbody *or* a power law in both the Q and the B modes (Mereghetti et al. 2013; hereafter M13).

Assuming the unpulsed radiation does not cease when the pulsed component is present, we infer that the additional thermal emission must have nearly 100% pulse fraction. However, since Deshpande & Rankin (2001) showed that all three axes of the pulsar (the observer line of sight, the rotation axis, and the magnetic dipole axis; see Fig. 1) are aligned within $\sim 10^\circ$, at first glance it appears unlikely that such a high pulse fraction can be achieved via the standard polar cap hot spot. In section 3 we demonstrate that, in fact, this problem is remedied by the inclusion of magnetic beaming.

H13 proposed that the strong pulsation may be explained by periodic obscuration of the X-ray emission via electron scattering in the magnetosphere. The resonant scattering cross-section σ for photons with frequency ω can be written as (e.g., Canuto et al. 1971)

$$\sigma = \frac{4\pi^2 e^2}{m_e c} |\varepsilon_-|^2 \delta(\omega - \omega_c), \tag{1}$$

where e and m_e are the electron charge and mass, respectively, and $\omega_c \equiv eB(r)/m_e c$ is the cyclotron frequency at a distance r from the neutron star (NS), and ε_- specifies the circular polarization (around the magnetic field) of the photon. We characterize the magnetosphere particle (electron or positron) number density $n(r)$ in terms of the Goldreich-Julian density, i.e., $n(r) \simeq \lambda_{\rm GJ}\Omega B(r)/(2\pi ec)$, with $\lambda_{\rm GJ}$ the multiplicity factor. Using $B(r) \simeq B_\star (R_\star/r)^3$ and $|\varepsilon_-| \simeq 1$, we find that the photon optical depth $\tau = \int_{R_\star}^{\infty} n\sigma dr$ is

$$\tau \simeq 10^{-3}\,\lambda_{\rm GJ} \left(\frac{P}{1\ {\rm sec}}\right)^{-1} \left(\frac{R_\star}{10\ {\rm km}}\right) \left(\frac{B_\star}{10^{12}\ {\rm G}}\right)^{\frac{1}{3}} \left(\frac{E}{1\ {\rm keV}}\right)^{-\frac{1}{3}}, \tag{2}$$

where P, $R_\star$, and $B_\star$ are the period, radius, and surface magnetic field of the pulsar, and $E = \hbar\omega$ is photon energy. For the range of photon energies of $0.2 - 2$ keV in which the X-ray pulsation is observed, in order for sufficient obscuration to occur ($\tau \gtrsim 1$), the density of the plasma must be about 1000 times the Goldreich-Julian density. While theoretically possible, it is unclear such a large particle density can be achieved in the closed magnetosphere region. Observationally, many isolated NSs (including both active radio pulsars and pure thermally emitting sources) have detectable X-ray emission from the whole stellar surface (e.g., Kaspi et al. 2004; Zavlin 2007), indicating that obscuration of surface X-rays by the magnetosphere is not significant.

The second puzzle of PSR B0943+10 is the presence of "drifting subpulses" in its radio emission (Deshpande & Rankin 2001). These drifting subpulses are thought to be a consequence of $\mathbf{E}\times\mathbf{B}$ drifting of a pattern of "sparks" in the polar cap accelerator of the NS (Ruderman & Sutherland 1975; Ruderman & Gil 2006). This implies the presence of a "vacuum gap" - a region directly over the polar cap in which the pulsar magnetosphere has pulled away from the surface of the NS, leaving a gap in which no plasma is present[5]. This gap then has a strong voltage drop across it, acting as an accelerator for charged particles and causing them to emit high-energy radiation, which later decays into highly bunched radio emission via a pair-production cascade a few tens of NS radii away from the surface. The presence of this gap is usually predicated upon the inability of ions to become dissociated from the NS surface. According to the electronic structure calculations of condensed matter in strong magnetic fields by Medin & Lai (2006), for an iron NS surface, a high surface magnetic field ($\gtrsim 10^{14}$ G, see Fig. 7 of Medin & Lai 2007) is required to keep the ions bound to the surface. The required field strength is even larger if the condensed surface is made of lighter elements (C or He). On the other hand, the surface dipole magnetic field inferred from the P-$\dot{P}$ measurement of PSR B0943+10 is a modest 2×10^{12} G, which is certainly insufficient for a gap to form. This implies that perhaps the local surface magnetic field at the polar cap of the NS is much higher than the dipole field inferred from P-$\dot{P}$.

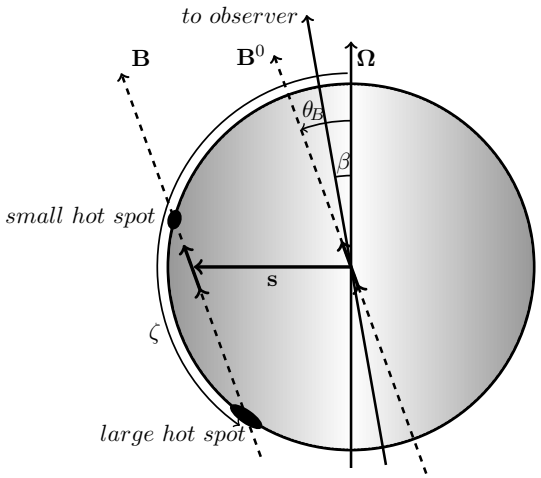

FIG. 1.— A schematic picture of the emission geometry of PSR B0943+10, and the proposed displaced dipole model of section 4. The misalignment of axes is exaggerated for clarity. The angles (β, θ_B) have been constrained by Deshpande & Rankin (2001) to be in the range between $(7^\circ, 11^\circ)$ and $(9^\circ, 15^\circ)$.

Finally, the fitted emission area of the thermal hot spot (M13) is found to be much smaller ($20 - 30$ m) than the canonical polar cap size, $R_{\rm cap} = R_\star\sqrt{R_\star\Omega/c} = 140$ m. In sections 3 and 4 we demonstrate that, with proper atmospheric modeling, the emission area can be consistent with the polar cap size.

3. LIGHT CURVES AND THE CANONICAL EMISSION GEOMETRY

H13 found that the pulsed component of the X-ray emission during the Q mode is comprised of a thermal blackbody that has a pulse fraction close to 100%. As discussed in Sec. 2, this poses a challenge to models of emission from a standard polar cap hot spot. However, the determination of the pulse fraction is uncertain. H13 showed the pulse fraction (before subtracting the unpulsed flux) to be $10\% \pm 15\%$ at 0.2-0.5 keV, and thus the pulse fraction at low energies can be low and is even consistent with zero.

[5] It is well known that a full vacuum gap potential would lead to too fast drifting subpulses, so a partially screened gap may be required (e.g., Gil, Melikidze & Geppert 2003; van Leeuwen & Timokhin 2012). See also Jones (2014) for an alternative model for drifting subpulses in pulsars.

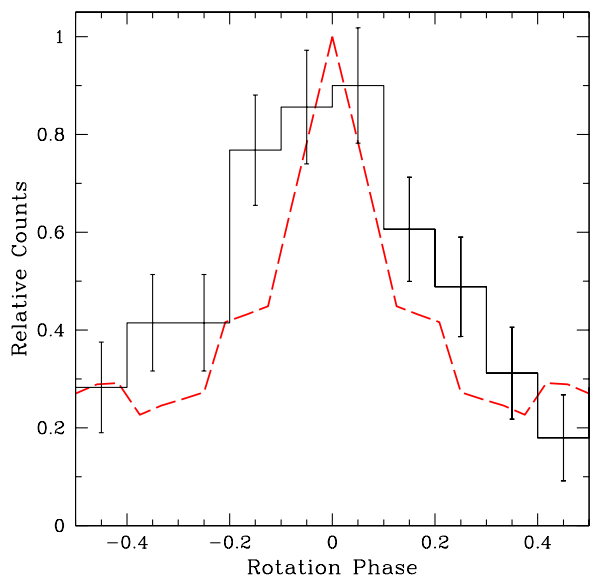

FIG. 2.— Q mode X-ray pulse profile of PSR B0943+10. The histogram is the observed (0.15–12 keV) pulse profile taken from Fig. 3 of M13, where we subtracted the background counts and normalised by the maximum. Errors are $\approx 1\sigma$. The dashed curve is the result of our atmosphere model with $B = 2 \times 10^{12}$ G, $M = 1.2\,M_\odot$ and $R_\star = 12$ km ($1 + z = 1.19$), $R_{\rm em} \approx 85$ m, $T_{\rm eff} = 1.5 \times 10^6$ K, and $(\beta, \theta_B) = (8^\circ, 14^\circ)$.

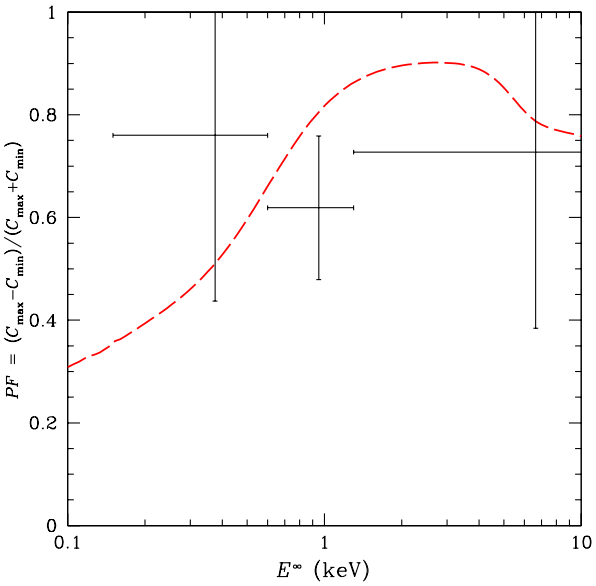

FIG. 3.— Q mode X-ray pulse fraction as a function of energy for PSR B0943+10. The observed pulse fraction (crosses) are calculated from the pulse profiles shown in Fig. 3 of M13 after subtracting the background counts, and errors are $\approx 1\sigma$. Dashed curve is the (redshifted) result of our atmosphere model (see Fig. 2 for model values).

This is supported by the analyses of M13 who found (by fitting the pulse profiles with a constant plus sinusoid) pulse fractions of $66\% \pm 13\%$, $56\% \pm 8\%$, $53\% \pm 13\%$ at 0.15-0.6 keV, 0.6-1.3 keV, and 1.3-12 keV, respectively. We also see from Fig. 3 of M13 that the [(max-min)/total] pulse fractions are $\approx 40 - 100\%$, $\approx 45 - 75\%$, and $\approx 35 - 100\%$, respectively, accounting approximately for the 1σ errors in the pulsed and background components (see Figure 3).

Since these pulse fractions may be less than 100%, we now attempt to obtain standard polar cap hot spot solutions that are consistent with the observed spectrum, pulse fraction, and pulse profile of PSR B0943+10. We employ a magnetized partially ionized hydrogen atmosphere model (Ho et al. 2008) to generate X-ray spectra and pulse profiles with a procedure that accounts for relativistic effects (Ho 2007). We take a magnetic field of 2×10^{12} G (the dipole field inferred from P and $\dot{P}$) that is directed perpendicular to the surface normal. We denote by β the angle between the line of sight and the rotation axis, and by θ_B the angle between the magnetic and rotation axes (see Figure 1). We assume $\beta = 7 - 9^\circ$ and $\theta_B = 11 - 15^\circ$, as constrained by Deshpande & Rankin (2001), and NS mass and radius $M = 1.2\,M_\odot$ and $R_\star = 12$ km, so that the gravitational redshift is $1 + z = 1.19$. Whether we include or neglect an antipodal hot spot has no effect on our results since this second hot spot is not visible for the assumed viewing geometry and gravitational redshift. Here we describe our approximate fits, leaving detailed fits for future work with higher-quality data.

We find that an atmosphere with $T_{\rm eff} \approx (1.4 - 1.5) \times 10^6$ K and emission radius $R_{\rm em} \approx 85$ m matches qualitatively the radio-quiet X-ray spectrum of PSR B0943+43 from H13. Previous blackbody fits find $T_{\rm BB} = 3 \times 10^6$ K and $R_{\rm BB} \approx 20 - 30$ m (H13, M13); note that the lower temperature and larger emitting area are typical characteristics of atmosphere emission compared to blackbody emission (see, e.g., Romani 1987; Shibanov et al. 1992). The atmosphere emission radius (85 m) is much closer to that expected for a centered dipole (140 m) than the blackbody emission radius. Figures 2 and 3 show examples of our atmosphere model results for the pulse profile and pulse fraction compared to the measurements of M13 (errors are calculated from the square root of the number of counts; c.f. Gehrels 1986). We see that the atmosphere model shows promise, as long as the low-energy pulse fraction is indeed $< 100\%$.

4. LIGHT CURVES AND THE DISPLACED DIPOLE GEOMETRY

In the previous section, we allowed for the low-energy pulse fraction of the Q-mode emission to be relatively low. If future observations of PSR B0943+10 show that the pulse fraction is high across all energy bands, then the "canonical" model of Sec. 3 cannot work. We thus explore an alternative model for the emission geometry, in which the magnetic dipole axis is displaced by a vector $\mathbf{s}$ from the center, such that θ_B is unchanged and thus the radio emission geometry and polarization profile are not altered (see Fig. 1), assuming that the radio emission originates beyond a few tens of NS radii away from the surface.

Displaced magnetic dipoles have been invoked before to explain various phenomena exhibited by pulsars. For example, Arons (2000) demonstrated that the position of the pulsar death line can be altered by displacing the magnetic dipole, and that to explain all observed active pulsars displacements of as much as $(0.7 - 0.8)R_\star$ are needed. More recently, Burnett & Melatos (2014) showed that a displaced magnetic dipole may explain some anomalies exhibited by the $Q-U$ phase portraits of some radio pulsars.

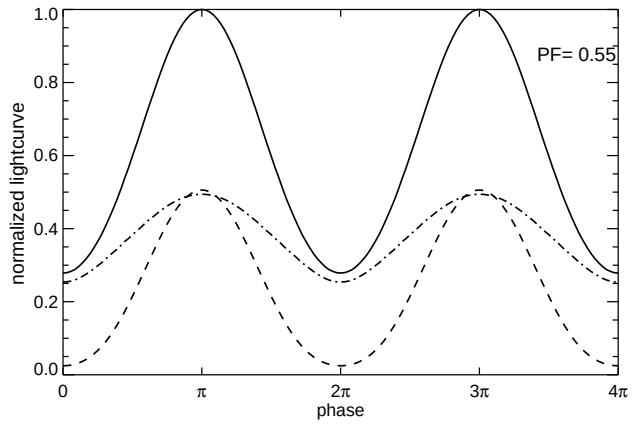

FIG. 4.— Theoretical light curves for the displaced-dipole model of PSR B0943+10 at (0.2−12)keV. See Fig. 1 for a schematic representation of the model; here, $\zeta = 125°$, and $(\beta, \theta_B) = (7°, 11°)$. Each hot spot has $T_{\rm eff} = 1.5 \times 10^6$K; the magnetic fields are 2×10^{14}G and 2.7×10^{12}G for the near and far spots, respectively. The dot-dashed curve shows the B-mode light curve due to the near spot with a pulsation of 31%. The dashed curve shows the emission from the far spot, visible only in the Q mode. The solid curve – the sum of the near and far spots– is the total Q mode light curve, with a pulsation of 55%.

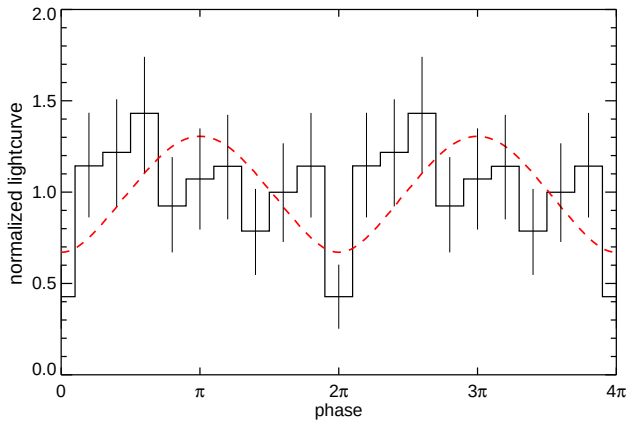

FIG. 5.— Observed (solid histogram) and theoretical (red dashed) light curves for B mode X-ray emission of PSR B0943+10 at (0.2 − 12)keV. The histogram is taken from Fig. 4 of M13. Errors are $\approx 1\sigma$. Both the histogram and the theoretical curve have been normalized by their respective mean values. All parameters are same as those of Fig. 4, but we assume that in the B mode only the small spot is visible.

We consider a $M = 1.4M_\odot$, $R_\star = 10$ km NS with a dipole surface magnetic field $B_d \simeq 2 \times 10^{12}$ G and propose the following scenario: (i) *All* or most of the X-ray emission from PSR B0943+10 is thermal in nature, which is, to date, consistent with the analyses of the X-ray spectra carried out by H13 and M13. (ii) The magnetic dipole axis is transposed such that both polar cap hot spots are potentially visible, as shown in Figure 1. The larger (far) spot has a lower magnetic field, while the smaller (near) spot has a larger magnetic field. In the Q mode, the large spot comes close to being invisible (note that the strong light bending effects enable the surface hot spots to be observed up to 135° from the line of sight), and thus produces a nearly-100% pulsation. The observed Q mode X-ray light curve is then composed of the nearly-constant emission from the near spot, and the strongly pulsed emission from the far spot. (iii) The transition from the Q mode to the B mode involves a small shift in the magnetosphere or the dipole axis, such that the large spot – which is already close to being unseen – becomes completely invisible, leaving only the nearly-constant light curve of the small spot.

We denote by ζ the angle between the rotation axis and the large polar cap (see Fig. 1). Quite naturally, the only way to produce a thermal light curve with a 100% pulse fraction across *all* energy bands is through geometry: a hot spot must be placed such that it is close to becoming invisible, in the range $\zeta \in (125°, 135°)$. Then the possible magnetic field axis orientations are constrained to a conical shell of width $2\theta_B$ centered on the hot spot. However, since the observed peaks of X-ray and radio emissions from PSR B0943+10 are in phase (H13), the magnetic axis must be oriented as shown in Fig. 1. It follows that the dipole must be displaced by a distance s $\approx (0.85-0.9)R_\star$, though its precise position, as well as the effective temperatures of each hot spot, remain unknown. We do not attempt to explore this parameter space. Rather, we present one test case to demonstrate that, in principle, all the X-ray observations of PSR B0943+10 can be explained by this model.

Naturally, the smaller "near" spot must be the source of the radio emission. As discussed in section 2, the presence of drifting subpulses in the radio emission likely implies the presence of a vacuum gap at the hot spot surface, and a strong ($\gtrsim 10^{14}$G) surface magnetic field is required to create such a gap. Therefore, we place the magnetic dipole close to the surface of the near spot.

We use the method ("Temperature Template with Full Transport", or TTFT) developed in Shabaltas & Lai (2012) to compute synthetic light curves for our chosen hot spot configuration. The TTFT method uses temperature profiles (as a function of depth) of magnetic NS atmospheres to efficiently compute the observed surface thermal radiation, taking into account the effects of magnetic atmosphere opacities, beam pattern, vacuum polarization, and gravitational light bending. For this work, we have used realistic ionized hydrogen magnetic NS atmosphere models (Ho & Lai 2001,2003) to calibrate our temperature profiles for the relevant effective temperature and surface magnetic field values.

As the blackbody fits of both the B mode and the Q mode spectra are very similar, we fix the two hot spots to have equal temperature, $T_{\rm eff} = 1.5 \times 10^6$K. We fix the magnetic field strengths to be 2×10^{14}G and 2.7×10^{12}G for the small and large spots, respectively; it follows that the hot spot radii must be ≈ 20m and ≈ 100m. Figure 4 presents our results.

Satisfactory agreement with the Q mode observation is achieved. However, the B mode light curve in this particular case is not entirely constant; it has a pulse fraction of 31%, coming mostly from the lower-energy part of the emission. We note that this pulse fraction is within the 3σ upper limit (i.e., $\lesssim 50\%$) derived by M13 for the B mode pulse fraction. Figure 5 shows that the B mode theoretical lightcurve is consistent with the most up-to-date observations. We speculate that a careful search in the available phase space can reduce this pulsation, though it is not likely to disappear entirely.

5. DISCUSSION AND CONCLUSION

The simultaneous radio and X-ray observations of the mode-switching pulsar PSR B0943+10 provide a unique

opportunity for understanding this class of objects. In this paper, we have examined several puzzles presented by PSR B0943+10. Our conclusions can be summarized as follows.

We show that the large X-ray pulse fraction of the additional thermal component observed in the radio Q mode can be adequately reproduced by using the canonical emission geometry of PSR B0943+10, that is constrained by radio observations, and taking into account beaming due to a strong surface magnetic field. We find that the low-energy pulse fraction produced by this model is small ($\sim 50\%$).

We also consider another, more extreme, magnetic field geometry that is consistent with various observations, including the possibility that the extra thermal component has high pulse fractions in all energy bands. We show that by displacing the magnetic dipole by a large amount ($\sim 0.85 - 0.9R_\star$) from the center of the star, both the B and the Q mode X-ray observations can be explained as thermal emission coming from the magnetic polar caps, one of which is small in size and has a large surface magnetic field, thus being responsible for the radio emission, while the other is large in size and has a lower magnetic field and acts as the highly pulsed thermal component observed in the Q mode. We speculate that, when the pulsar is radio bright, the larger spot becomes invisible, leaving only the smaller spot's emission to be observed.

Overall, the models explored in this paper can be tested by future X-ray observations (e.g., the "extreme" model requires that most of the observed X-rays are thermal in nature and predicts a $\sim 30\%$ pulse fraction even in the B-mode). These will be valuable for constraining the magnetosphere plasma density and the magnetic field strength and geometry of PSR B0943+10, and will thereby further our understanding of the enigmatic behavior of pulsar mode switching.

W.C.G.H. appreciates the use of the computer facilities at KIPAC. This work has been supported in part by NSF grants AST-1008245, AST-1211061 and NASA grant NNX12AF85G.

REFERENCES

Arons, J. 2000, in Kramer M., Wex N., Wielebinski R., eds, ASP Conf. Ser. Vol. 202, IAU Colloq. 177: Pulsar Astronomy 2000 and Beyond. Astron. Soc. Pac., San Francisco, p. 449
Burnett, C.R., & Melatos, A. 2014, MNRAS, 440, 2519
Camilo, F., Ransom, S. M., Chatterjee, S., Johnston, S., & Demorest, P. 2012, ApJ, 746, 63
Canuto, V., Lodenquai, J., & Ruderman, M. 1971, Phys. Rev. D 3, 2303
Cordes, J.M. 2013, ApJ, 775, 47
Deshpande, A. A., & Rankin, J. M. 2001, Mon. Not. R. Astron. Soc. 322, 438
Dyks, J., Zhang, B., & Gil, J. 2005, ApJ, 626, L45
Gehrels, N. 1986, ApJ, 303, 336
Gil, J., Melikidze, G. I., & Geppert, U. 2003, A&A, 407, 315
Hermsen, W., Hessels, J. W. T., Kuiper, L., et al. 2013, Sci, 339, 436
Ho, W.C.G. 2007, MNRAS, 380, 71
Ho, W.C.G., & Lai, D. 2001, MNRAS, 327, 1081
Ho, W.C.G., & Lai, D. 2003, MNRAS, 338, 233
Ho, W.C.G., Potekhin, A.Y., & Chabrier, G. 2008, ApJS, 178, 102
Jones, P.B. 2014, MNRAS, 437, 4027
Kaspi, V.M., Roberts, M.S.E., Harding, A.K. 2004, in "Compact Stellar X-ray Sources", eds. W.H.G. Lewin and M. van der Klis (Cambridge U. Press) (arXiv:astro-ph/0402136)
Kramer, M., Lyne, A. G., OBrien, J. T., Jordan, C. A., & Lorimer, D. R. 2006, Sci, 312, 549
Lorimer, D. R., Lyne, A. G., McLaughlin, M. A., et al. 2012, ApJ, 758, 141
Lyne, A., Hobbs, G., Kramer, M., Stairs, I., Stappers, B.W. 2010, Science, 329, 408
Medin, Z., & Lai, D. 2006, Phys. Rev. A 74, 062508
Medin, Z., & Lai, D. 2007, MNRAS, 382, 1833
Mereghetti, S., Tiengo, A., Esposito, P., & Turolla, R. 2013, MNRAS, 435, 2568
Rafikov, R.R., & Goldreich, P. 2005, ApJ, 631, 488
Rankin, J. M., & Suleymanova, S. A. 2006, Astron. Astrophys. 453, 679
Romani, R.W. 1987, ApJ, 313, 718
Ruderman, M., & Gil, J. 2006, A&A, 460, L31
Ruderman, M. A., & Sutherland, P. G. 1975, ApJ, 196, 51
Shabaltas, N., & Lai, D. 2012, ApJ, 748, 148
Shibanov I. A., Zavlin, V. E., Pavlov, G. G., & Ventura, J., 1992, A&A, 266, 313
van Leeuwen J., & Timokhin A. N. 2012, ApJ, 752, 155
Zavlin, V.E. 2007, in Neutron Stars and pulsars, ed. W. Becker, Astronomy and Space Science Library, 357, 181-209 (arXiv:astro-ph/0702426)
Zhang, B., Gil, J., & Dyks, J. 2007, MNRAS, 374, 1103